PROCEEDINGS, Twenty-Eighth Workshop on Geothermal Reservoir Engineering
Stanford University, Stanford, California, January 27-29, 2003
SGP-TR-173

INFERRED WATER SATURATION IN THE GEYSERS BASED ON WELL PERFORMANCE DATA

Jericho L. P. Reyes and Roland N. Horne

Stanford Geothermal Program
Stanford University
Stanford, CA, U.S.A. 94305
e-mail: jlpreyes@stanford.edu, horne@stanford.edu

ABSTRACT

Available historical data from 503 wells at the Geysers geothermal field were analyzed to estimate in-situ water saturation in the reservoir. The pressure and temperature performance data of most of the wells demonstrate "dry-out" due to the formation of superheated steam. The in-situ water saturation of the reservoir can be inferred by using zero-dimensional models derived from mass and energy conservation equations. Techniques to identify the initial reservoir temperature and the dry-out temperature were developed and used in the saturation calculations. Effects of reinjection of the Geysers were analyzed and compared to models of depleted reservoirs. Regional trends of the saturation values plotted in the Cartesian plane were also investigated.

INTRODUCTION

The Geysers geothermal field in Northern California is the largest producing vapor-dominated field in the world. The exploitation of the geothermal reservoir entails the extraction of thermal energy, which is then used to generate electricity. Accurate knowledge of the parameters involved in this recovery process is of substantial economic value in making most effective use of the resource.

Exploitation of a geothermal field is dependent on the quantity of heat available in the reservoir and on how long it can be extracted (Bowen, 1989). Recovery of energy from a geothermal reservoir requires that mass be withdrawn from it. Once a reservoir has reached its maximum exploitative capacity, no more fluid can be extracted unless additional recharge liquid is injected into the reservoir artificially. Understanding when fluid will be exhausted and how much remains at any moment are important to predicting the ultimate recovery of the resource.

The basic components of a vapor-dominated geothermal reservoir are its reserves of steam and immobile water. Under exploitation the vapor-dominated field can be locally depleted of water to form a dry or superheated zone. There is a recharge of steam from boiling of the immobile water. Even though the steam is the principal recovery fluid, by mass the immobile water represents a much larger component of the reservoir fluid than the steam. Hence quantifying the immobile water in the reservoir is of particular importance.

Knowledge of the immobile and in-situ water saturation will also provide better understanding of the fluid storage capacities of geothermal rocks, as this is valuable in estimating the performance of a geothermal reservoir and its capacity for further exploitation.

BACKGROUND

Past projects have relied on numerical simulation to infer field conditions. Similar techniques have also been used to infer flow and saturation properties from experimental measurements. Belen and Horne(2000) used numerical simulation to verify values of in-situ and immobile water saturations calculated from zero-dimensional models based on those described in Grant, Donaldson and Bixley (1982). The principal objective of this study was to use Belen's model to match field data from the Geysers and thereby estimate the immobile water saturation.

The Geysers Geothermal Field is located in Northern California about 130 km north of San Francisco. Since 1987, The Geysers has experienced a decline in steam pressure (Barker and Pingol, 1997). Recovering some of the reduced reservoir capacity has been achieved by injecting water into parts of The Geysers reservoir to recover additional heat.

The Geysers production database was made available by the California Division of Oil, Gas and Geothermal Resources. The Geysers database, which contains temperature and pressure values for 502 wells around The Geysers field area, also contains information on the history and overall structure of the wells. As an illustrative example, the first sections this paper will describe a typical well from The Geysers database, namely McKinley 1, a redrilled active producer well, which has a depth of 2219.18 feet. The overall study considered all 502 of the

wells in the database, the results of which we will be discussed in later sections.

METHOD

The pressure-temperature profile of the example well, gathered over a period of 20 years, is plotted against the steam saturation curve and shown in Figure 1.

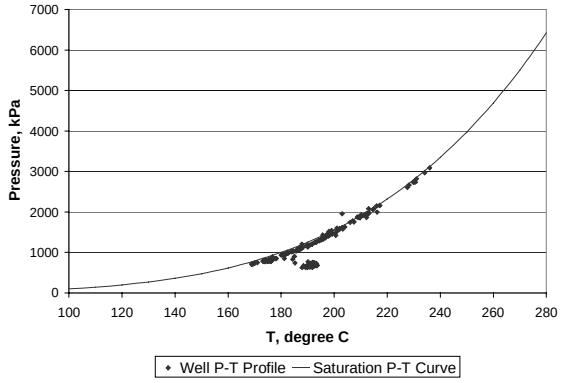

Figure 1: Pressure-temperature profile of the McKinley 1 well.

The well pressure-temperature profile suggests a clear relationship with the saturation pressure temperature curve of water. A noticeable deviation is the formation of a cluster at the lower pressure values under the saturation curve. The formation of this "elbow" in the pressure-temperature profile, in which the pressure values are lower than the saturated values for a certain temperature, can be attributed to the point in the exploitation history at which the immobile saturation of the water in the reservoir has been boiled away. The immobile saturation of the water is liquid that cannot flow in the reservoir, and hence represents an "invisible" phase. Nonetheless, the immobile water will become steam during exploitation, due to boiling, and hence is a very important source of energy.

To better understand when this phenomenon happens, we plotted the histories of the well over the same 20-year span. The result is shown in Figure 2.

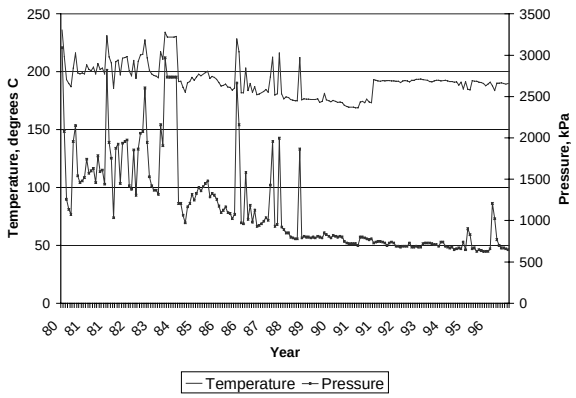

Figure 2: Temperature and pressure values over a 20-year exploitation period for the McKinley 1 well.

It can be seen in the left side of Figure 2 that the temperature fluctuates in the same manner as the pressure, or when the pressure goes up, the temperature goes up too. This trend is noticed from years 1980 to 1991. After a brief leveling off, the trend goes the opposite way, or when the temperature goes down, the pressure goes up and vice versa. Whether or not these phenomena are attributable to the point in the reservoir exploitation where the immobile water saturation has boiled away is examined in the following sections.

Previous Results in Simulation and Modeling

In 2000, Belen developed a two-phase radial reservoir model to determine the end-point saturation of steam and liquid water relative permeability curves by inference from pressure, temperature and saturation data. The objective of the study was to determine the end-points based on both zero-dimensional models and from numerical simulation.

Zero-Dimensional Model

Geothermal reservoirs under exploitation can be modeled using zero-dimensional models derived from material and energy conservation equations and Darcy's Law. Using the characteristics of vapor-dominated reservoirs, which primarily is the classification of The Geysers, where the mobile phase is steam, Darcy's Law describes the steam flow.

$$\phi \frac{\partial}{\partial t}\{s\rho_w + (1-s)\rho_s\} = -\nabla \cdot (u_s \rho_s) \quad (1)$$

$$\frac{\partial}{\partial t}\{(1-\phi)\rho_r c_r T + \phi(1-s)\rho_s h_s\} = -\nabla \cdot (u_s \rho_s h_s) \quad (2)$$

$$u_s = \frac{k k_{rs}}{\mu_s} \nabla p \quad (3)$$

The enthalpy of saturated steam is nearly constant with temperature under reservoir conditions. This

allows the simplification of the energy conservation equation relating pressure and saturation.

$$(1-\phi)\rho_r C_r T + \phi s \rho_w (h_w - h_s) = \text{constant} \qquad (4)$$

This zero-dimensional model allows us to calculate the in-situ water saturation using rock and fluid properties,

$$s_o = \frac{(1-\phi)}{\phi} \frac{\rho_r c_r (T_o - T_d)}{\rho_w (h_s - h_w)|_{T_o}} \qquad (5)$$

where T_o is the initial reservoir temperature and T_d is the dry-out temperature.

TOUGH2 Two-Phase Radial Flow Model

A two-phase radial flow was modeled using the numerical simulator TOUGH2 (Pruess, 1991). A cylindrical model was used in the simulation runs. A single well was placed in the middle of the reservoir. Table 1 summarizes the parameters used for the runs.

Table 1: Reservoir properties used in the simulation of the two-phase radial model.

Porosity	5%
Permeability	1×10^{-13} m^2
Rock Density	2600 kg / m^3
Rock Specific Heat	485 J / kg ºC
Reservoir Radius	1000 m
Reservoir Thickness	10 m
Initial Reservoir Temperature	280 ºC

The model consisted of 100 grid blocks, with grid size increasing logarithmically from the center to the boundary of the reservoir.

Figure 3 compares the production enthalpies simulated by TOUGH2 with those predicated by the zero-dimensional model with in-situ water saturation of 0.3. There is good agreement between the simulator and the model results. The zero-dimensional model simulated reservoir temperatures satisfactorily in comparison to the values computed with TOUGH2. Therefore, it is reasonable to use the zero-dimensional model to analyze the data taken from actual wells in The Geysers geothermal field. It should be noted that the ability of a volume-averaged model to replicate the fully dimensional result justifies the application to the Geysers, which is admittedly a heteregoneous and fractured reservoir. The pressure-temperature history data from the Geysers is analyzed over long periods (e.g. 20 years), during which time the bulk behavior is not expected to be governed by fractures and heterogeneities.

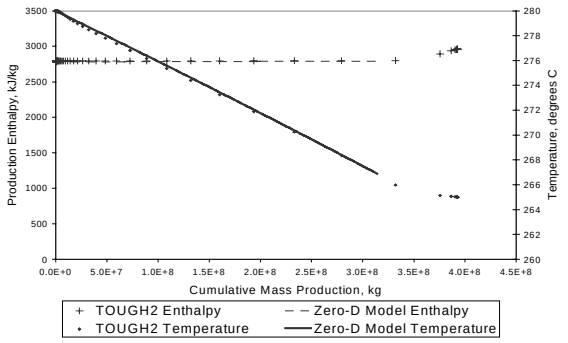

Figure 3: Production enthalpy and reservoir temperature profiles: initial water saturation = 0.3, irreducible water saturation = 0.3 (Belen, 2000).

Numerical Simulation of Pressure-Temperature Profiles

Using the two-phase radial model developed by Belen, and using the parameters given in Table 1, TOUGH2 simulations were made and pressure-temperature profiles were plotted. This is shown in Figure 4, with irreducible water saturation taken as 0.3.

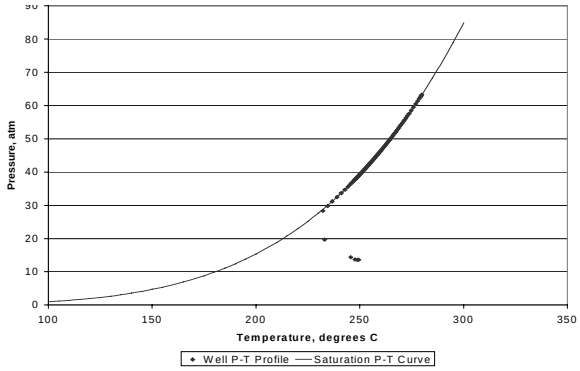

Figure 4: Pressure-temperature profile of the TOUGH2 simulated two-phase radial model, irreducible water saturation = 0.3.

The simulated values are in good agreement with the saturation curve, and the appearance of an elbow, similar to those seen in wells like McKinley 1, shows that when the reservoir reaches zero saturation, a lowering of pressure is observed as the well zone becomes superheated. Pressure values decrease and deviate from the saturation curve.

The history of the exploitation of the simulated reservoir is plotted in Figure 5 to better understand at what point this elbow occurs and if it is comparable with the actual well histories plotted in Figure 2.

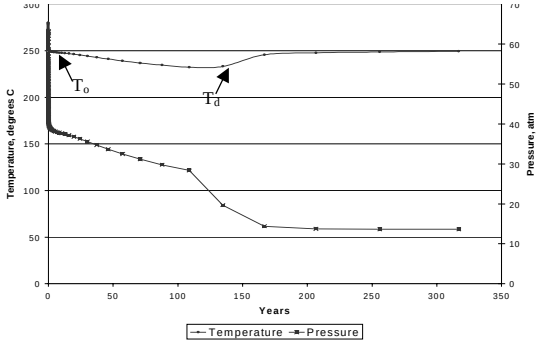

Figure 5: Temperature and pressure values over a 315 year exploitation period for the TOUGH2 simulated two-phase radial model, in-situ water saturation = 0.3.

The temperature and pressure histories from 0 to 100 years in Figure 5 are in direct relationship, that is, when pressure decreases, the temperature also decreases. After that, however, the opposite relationship exists, or as the temperature goes up, the pressure goes down. The point at which the behavior changes corresponds to the formation of the elbow in Figure 4, and is indicative of the reservoir reaching zero water saturation. This confirms the proposed explanation of the behavior of the McKinley 1 well, which reveals similar behavior.

To verify these results, we calculate the in-situ water saturation for the simulation run using Equation 5. From the equation, it is seen that two temperatures are needed for the calculation of s_o. The initial reservoir temperature, T_o, is used to evaluate the fluid properties ρ_w, h_s and h_w. The dry-out temperature, T_d, is determined to be the temperature just before the well reaches s_o.

$$s_o = \frac{(1-\phi)}{\phi}\frac{\rho_r c_r (T_o - T_d)}{\rho_w (h_s - h_w)\big|_{T_o}}$$

$$= \frac{(1-0.05)}{0.05}\frac{\left(2600\,{}^{kg}/_{m^3}\right)\left(0.485\,{}^{kJ}/_{kgC}\right)(250^oC - 232^oC)}{799.1689\,{}^{kg}/_{m^3}\left(2800.4\,{}^{kJ}/_{kg} - 1085.78\,{}^{kJ}/_{kg}\right)} = 0.31$$

The zero-dimensional model, as expressed in Equation 5 with reservoir properties used in Table 1, gives a close approximation (0.31) of the in-situ water saturation used in the simulation (0.30). This means that the assumptions taken in the zero-dimensional model can closely approximate the conditions in actual geothermal wells, therefore, this method was used to calculate the in-situ water saturation in the Geyser wells.

Estimation of the Initial Reservoir Temperature

Figure 2 shows that, with the temperature-pressure profile of The Geysers wells, unlike with the simulated results, the initial reservoir temperature, T_o, cannot be distinguished so easily. Taking into account the initial sudden drop in the downhole wellbore pressure as a response to production, the stable temperature, T_o, after the early transient period can be estimated by taking the median temperatures in the first few years. Figure 6 illustrates this estimation.

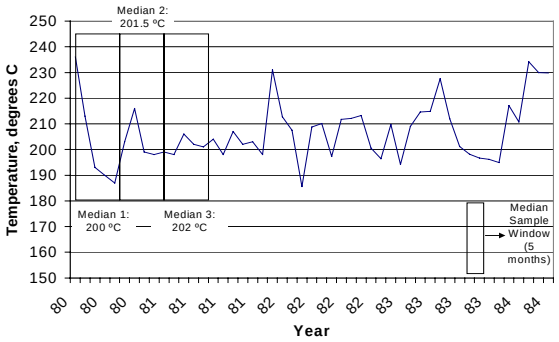

Figure 6: Estimation of the initial reservoir temperature T_o, using a median sample window of 5 months for McKinley 1. The estimated T_o is 201.5 ºC.

Estimation of the Dry-out Temperature

The dry-out temperature can be estimated by acknowledging the fact that this temperature is found where the direct relationship of the temperature and pressure ends, and where the inverse relationship begins, as observed in the determination of the T_d in the simulation case. To do this, we analyze Figure 1. The region of the pressure-temperature profile following the saturation curve corresponds to the period of direct relationship in the pressure and temperature values, and the values below the elbow correspond to the inverse relationship. Figure 7 illustrates the relationships that are present with pressure and temperature values, as seen in the computation of the correlation function *R*.

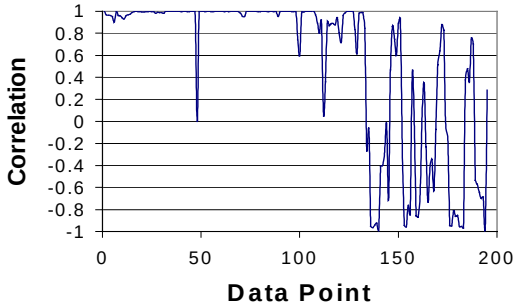

Figure 7: Calculation of the correlation between temperature and pressure data points for McKinley 1, using a five-point moving correlation window.

It can be seen from the figure that most of the left side of the graph has a positive correlation. The right side, on the other hand, fluctuates from positive to

negative correlation, although the relationship is largely inverse.

We can estimate this point numerically by recognizing that, at the values of positive correlation, the temperature and pressure values obey the saturation curve. The saturation curve values are generated using the Clausius-Clapeyron equation, given by Equation 6.

$$\ln p = -\frac{\Delta h_{vap}}{R_g T} + C \qquad (6)$$

This equation includes the Δh_{vap}, which is the heat of vaporization of water, and R_g, the universal gas constant. Therefore, we can estimate the time when the positive correlation zone ends, by analyzing the point at which the values of temperature and pressure history stop following the Clausius-Clapeyron equation.

Figure 8 shows the plot of the saturation pressure values computed from the corresponding historic well temperature values, in comparison to the historic pressure well values. We can see that there are points at which the well pressure values start to deviate from the saturated values, as indicated by the arrow. These points can be used to estimate the point of dry-out.

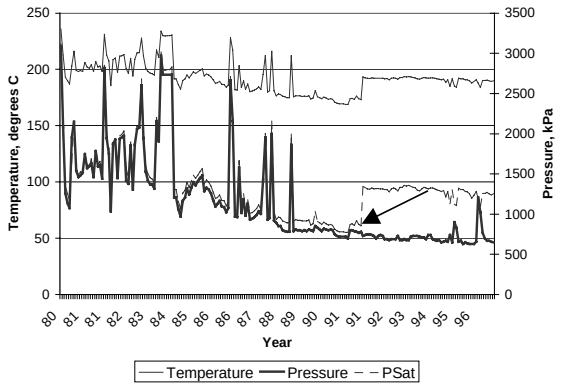

Figure 8: Saturated pressure values calculated from well temperature values and pressure values over a 20 year period for the McKinley 1 well.

The Clausius-Clapeyron equation can be plotted as a straight line by plotting ln(*p*) vs. 1/*T*. We can therefore extend this realization to the well data, assuming the elbow will not follow this straight line. Figure 9 illustrates this premise, with the first part of the well data generally agreeing with the linear relationship, and the second part, the elbow, deviating from the line. The point which separates these two parts will be the dry-out temperature, T_d.

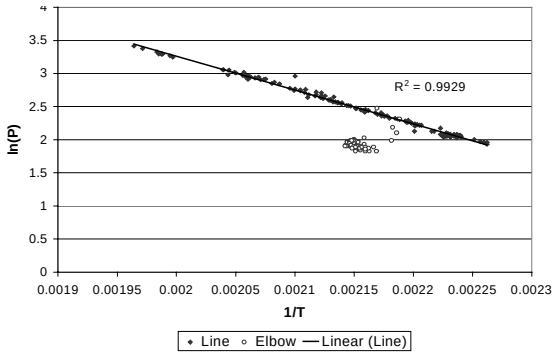

Figure 9: Plot of ln(p) vs. 1/T of the McKinley 1 pressure and temperature values to determine the dry-out temperature. The estimated T_d is 193.2 ºC.

CALCULATION OF THE IN-SITU WATER SATURATION

The in-situ water saturation values for The Geysers geothermal wells can then be calculated based on the T_o and T_d values and the assumed reservoir properties shown earlier in Table 1. Table 2 shows us the calculated values of the saturations, as well as the values for T_o and T_d used to arrive at this result. Figure 10 gives us a contour map of the calculated saturation values plotted over the XY plane. We have identified 177 wells in the database that have the presence of the dry-out point, therefore allowing the computation of the saturation values.

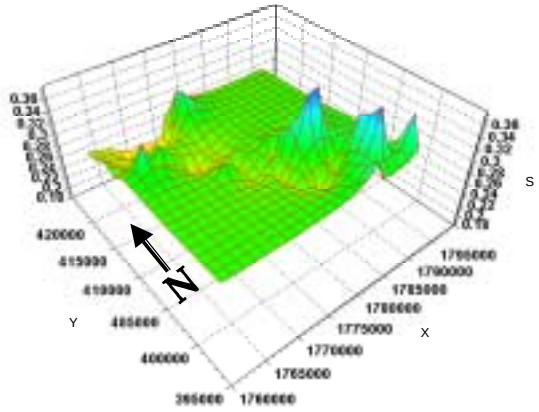

Figure 10: Contour plot of the saturation values computed for the T_o and T_d values of 177 Geyser wells with respect to the XY plane.

We also identified wells that do not have a discernable change in trend, and therefore infer that these wells have not reached superheat. Figure 11 shows an example of such a well, and as we can see the relationship between the pressure and temperature is direct all throughout the history. We have identified 147 wells that exhibit this trend.

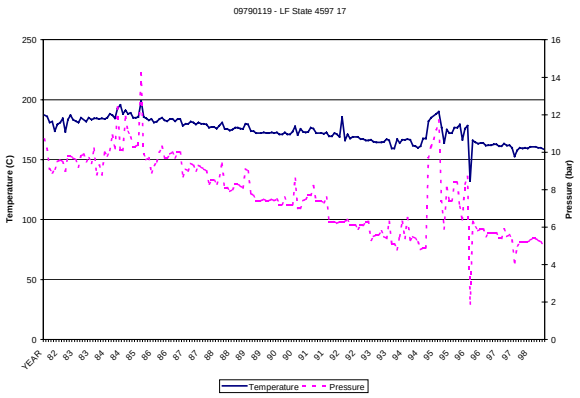

Figure 11. Temperature and pressure values over a 20-year exploitation period for a well with no dry-out point.

The remaining 179 wells have data that is too sparse to observe any relationships. An example of such a well is shown in Figure 12. We also have identified 25 injection wells from the database.

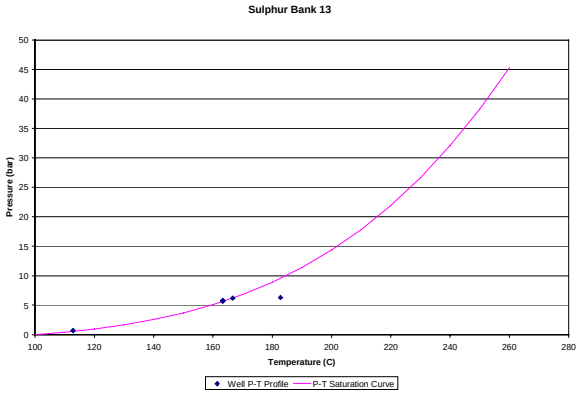

Figure 12: Pressure-temperature profile of a well with sparse data.

To understand the possible spatial trends the wells can take on considering their saturation values in relation to the Cartesian plane, we map out different types of wells we have classified. Figure 13 shows us an aerial view of the contour plot made by the saturation values. The two boxes located in the upper-left region of the plot, and the lower-left region of the plot correspond to the Northwest (NW) and Southeast (SE) zones, respectively. Figure 14 shows us the same plot, this time showing the individual locations of these wells. We can see that in the SE location, we have mostly blue colors, signifying a high saturation value (0.3 – 0.5). In the NW location, we see orange and yellow values, indicating that there is a concentration of low saturation values in this zone (0.15 – 0.25).

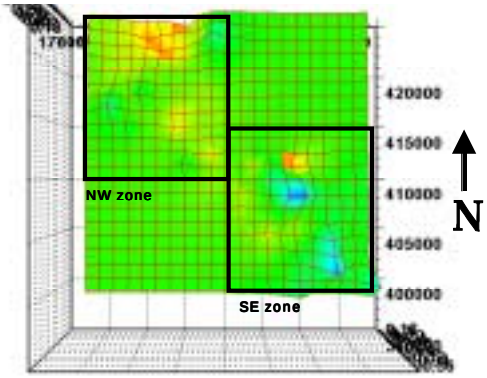

Figure 13: Aerial view contour plot of the saturation values on the Cartesian plane of the 177 superheated Geyser wells.

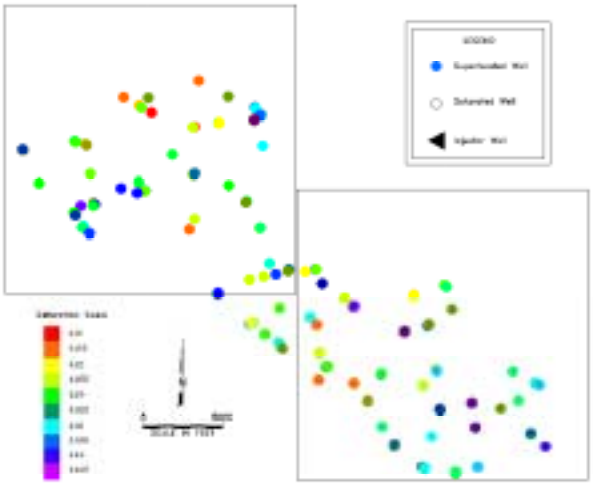

Figure 14: Plot of the XY locations of the superheated wells.

Figure 15 shows us the plot of wells that have not yet reached superheat, which we now call “saturated” wells, on the Cartesian plane. The NW zone has 64% of all the saturated wells, indicating that there is a higher number of saturated wells in the NW zone than in the SE zone.

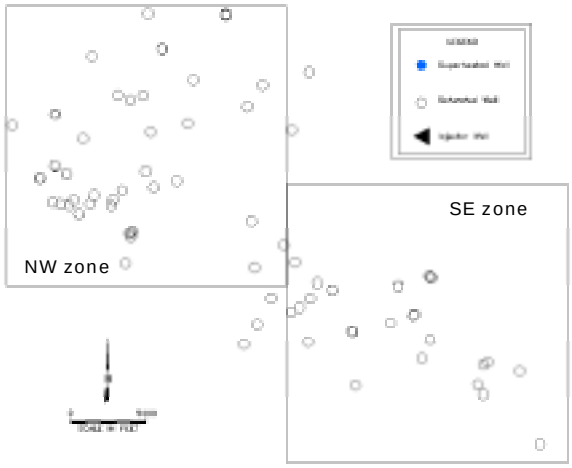

Figure 15: Plot of the XY locations of the saturated wells.

EFFECT OF REINJECTION

To investigate the possible effect of an increase of the calculated saturation values due to reinjection, we plotted the locations of the injection wells in the Cartesian plane. Figure 16 shows the plot, and we can say that these wells are evenly distributed throughout the field.

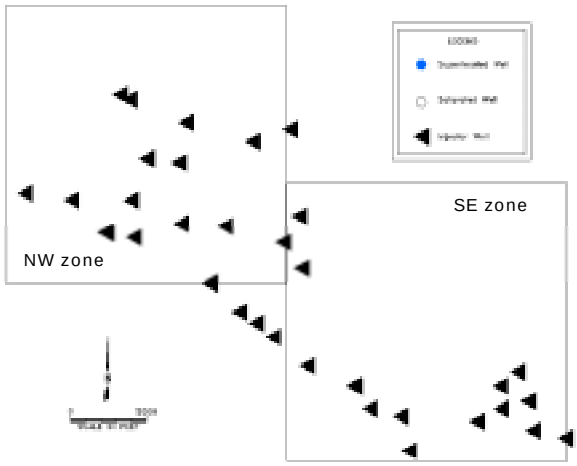

Figure 16: Plot of the XY locations of the injection wells.

We analyzed the trends presented so far further by simulating the influence of reinjection in the vicinity of producing well using TOUGH2. In the simulation, we injected water at constant flowrate and 20ºC temperature to the grid cell farthest from the center of the radial model that we have used in previous simulations. We used a value of 0.3 for the in-situ water saturation and we investigated whether reinjection affects the estimates of this value from the zero-dimensional model. The temperature and pressure profiles for this simulation are plotted in Figure 17.

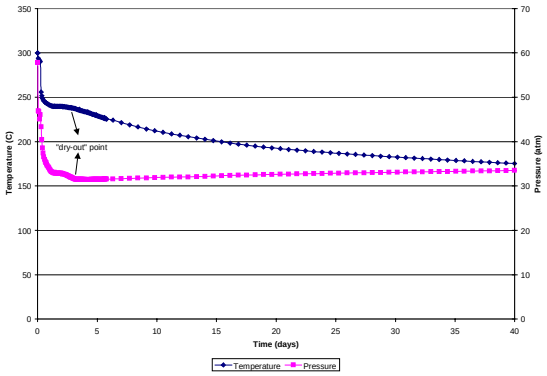

Figure 17: Pressure-temperature profile over a 40 day exploitation period showing the dry-out point for a simulation run showing reinjection.

In Figure 17, we have identified the zones of direct and inverse relationships, therefore we can use this to identify the T_o and T_d values to calculate the in-situ water saturation from our zero-dimensional model. As we can see from the calculation, the original saturation of 0.3 has appeared to increase to 0.36, indicating that indeed reinjection increases estimated value of the in-situ water saturation in the well.

$$s_o = \frac{(1-\phi)}{\phi}\frac{\rho_r c_r (T_o - T_d)}{\rho_w (h_s - h_w)\big|_{T_o}}$$

$$= \frac{(1-0.05)}{0.05}\frac{\left(2600\,{}^{kg}/_{m^3}\right)\left(0.485\,{}^{kJ}/_{kgC}\right)(256^\circ C - 235^\circ C)}{799.1689\,{}^{kg}/_{m^3}\left(2800.4\,{}^{kJ}/_{kg} - 1085.78\,{}^{kJ}/_{kg}\right)} = 0.36$$

We might therefore attribute the high saturation values found in the SE zone as a product of reinjection. It is know that in this zone, we have the presence of an enhanced water supply (from the Lake County waste water project), therefore this, coupled with a lowering of pressure in the zone, contributes to the high apparent saturation values. This also explains the presence of fewer saturated wells, as the wells were more likely to dry up in this zone than in the NW zone, prior to the enhanced injection.

CONCLUSIONS

Based on the present study, the following conclusions may be drawn:

1. Vapor-dominated geothermal reservoirs under exploitation can be depleted locally of water to form a dry or superheated zone.
2. Well performance data history can be used to infer in-situ water saturation.
3. A geothermal reservoir can be said to have dried-out when its pressure-temperature profile deviates from the steam saturation curve.
4. Zero-dimensional models can be used to calculate the in-situ water saturation after

identifying the initial reservoir temperature and the dry-out temperature.

5. Prior to exploitation, The Geysers wells had saturation values mostly in the range 0.3 to 0.5 in the Southwest zone. The wells in the Northwest zone had saturation values mostly in the 0.15 to 0.25 range.
6. An increase in apparent in-situ saturation is attributable to reinjeciton of water.

ACKNOWLEDGEMENTS

This work was funded by a PIER Grant by the California Energy Commission. We are also grateful for the assistance of the California Division of Oil, Gas and Geothermal Resources and Calpine Corporation.

REFERENCES

Barker, B., and Pingol, A.: "Geyser Reservoir Performance – An Update," *Proceedings*, Twenty Second Workshop on Geothermal Reservoir Engineering, Stanford University, California, Stanford, January 27-29, 1997; SGP-TR-155.

Belen, R.P., Jr.. and Horne, R.N.: "Inferring In-Situ and Immobile Water Saturations from Field Measurements", Geothermal Resources Council *Transactions* **24** (2000).

Bowen, R.: "*Geothermal Resources*," 2nd Edition, Elsevier Science Publishing Co., Inc, New York, 1989.

Grant, M., Donaldson, I., and Bixley, P.: "*Geothermal Reservoir Engineering*," Academic Press, Inc., New York, 1982.

Pruess, K.: "TOUGH2 - A General-Purpose Numerical Simulator for Multiphase Fluid and Heat Flow", Report LBL-29400, Lawrence Berkeley National Laboratory, Berkeley Calif. (1991).

Table 2: Saturation values for the 177 superheated wells and the T_o and T_d used to calculated them.

Well Name	So	To (ºC)	Td (ºC)	Well Name	So	To (ºC)	Td (ºC)
Abel 1	0.25	196	178.3	DX State 4596 60	0.33	197.2	173.9
Angeli 2	0.205	186.1	171.1	DX State 4596 62	0.157	183.3	171.7
Angeli 3	0.212	186.1	170.6	DX State 4596 68	0.255	192.2	173.9
Beigel 1	0.168	188.9	176.7	DX State 4596 69	0.323	197.2	174.4
Beigel 2	0.282	195.6	175.6	DX State 4596 73	0.191	188.3	174.4
Beigel 3	0.259	186.7	167.8	DX State 4596 74	0.174	185	172.2
CA-1862 15A-21	0.522	208.3	172.8	DX State 4596 75	0.222	188.3	172.2
CA-1862 15B-21	0.263	186.7	173.3	DX State 4596 76	0.365	198.9	173.3
CA-1862 62D-29	0.207	193.7	178.9	DX State 4596 82	0.168	185.6	173.3
CA-5634 21-12	0.241	191.7	174.4	DX State 4596 85	0.287	193.3	172.8
CA-5634 21A-12	0.27	192.2	172.8	Francisco 02-05	0.286	190.6	170
CA-5634 21B-12	0.231	190.6	173.9	GDC 1	0.246	190	172.2
CA-5634 21D-12	0.231	190	173.3	GDC 10	0.28	193.9	173.9
CA-5634 32-12	0.197	186.1	171.7	GDC 11	0.299	195.6	174.4
CA-5634 32A-12	0.269	191.1	171.7	GDC 19	0.238	190	172.8
CA-5634 32B-12	0.214	187.8	172.2	GDC 2	0.19	186.1	172.2
CA-5634 32C-12	0.198	187.2	172.8	GDC 20-29	0.281	194.4	174.4
CA-5634 45B-12	0.229	187.8	171.1	GDC 23	0.221	185.6	169.4
CA-5634 52-11	0.351	200.6	176.1	GDC 24	0.279	192.8	172.8
CA-5635 117-19	0.301	192.2	170.6	GDC 25	0.238	190	172.8
CA-5635 123-19	0.188	183.3	169.4	GDC 29	0.223	190	173.9
CA-5635 94A-19	0.255	190.6	172.2	GDC 32A-13	0.342	192.8	168.3
CA-5635 94B-19	0.37	197.2	171.1	GDC 66-12	0.342	194.4	170
CA-5636 23B-22	0.246	182.6	164.4	GDC 7	0.244	189.4	171.7
CA-5636 23G-22	0.271	187.6	167.9	GDC 85-12	0.257	185	166.1
CA-5636 23H-22	0.186	184.4	170.7	GDC 86-12	0.369	195.6	169.4
CA-5636 36C-22	0.216	181.9	165.9	GDC 9	0.223	190	173.9
CA-5636 68B-21	0.482	196.6	162.5	Geyser Gun Club 6	0.247	193.3	175.6
CA-5636 68D-21	0.521	197.9	161.2	Geyser Gun Club 8	0.201	190.6	176.1
CA-5636 74G-21	0.193	177.8	163.3	Happy Jack 11	0.213	185.6	170
CA-5636 74H-21	0.185	177.4	163.5	LF State 4597 1	0.286	192.2	171.7
CA-5636 87A-21	0.219	180.5	164.2	LF State 4597 10	0.385	195.6	168.3
CA-5636 87B-21	0.309	182.3	159.4	LF State 4597 12	0.213	185	169.4
CA-5636 87C-21	0.305	182.9	160.4	LF State 4597 13	0.227	185	168.3
CA-5636 87D-21	0.489	197.4	162.9	LF State 4597 14	0.219	185	168.9
CA-5636 87G-21	0.309	186.3	163.7	LF State 4597 18	0.279	192.8	172.8
CA-5637 68-21	0.408	193.8	164.7	LF State 4597 27	0.206	187.2	172.2
CA-5639 14A-27	0.207	201.1	186.7	LF State 4597 28	0.255	190.6	172.2
CA-5639 15-28	0.301	191.1	169.4	LF State 4597 29	0.222	188.3	172.2
CA-5639 15A-28	0.251	187.2	168.9	LF State 4597 31	0.213	185	169.4
CA-5639 15C-28	0.158	181.7	170	LF State 4597 34	0.27	192.2	172.8
CA-5639 15D-28	0.174	180.6	169.4	LF State 4597 36	0.238	189.4	172.2
CA-5639 36-28	0.196	181.7	167.2	LF State 4597 37	0.341	193.3	168.9
CA-5639 42-33	0.267	186.7	167.2	LF State 4597 38	0.188	182.2	168.3
CA-5639 44-28	0.253	190	171.7	LF State 4597 4	0.309	190.6	168.3
CA-5639 44A-28	0.259	187.2	168.3	LF State 4597 42	0.214	187.8	172.2
CA-5639 44B-28	0.319	193.9	171.1	LF State 4597 48	0.159	183.9	172.2
CA-5639 53-33	0.327	192.8	169.4	LF State 4597 49	0.174	185	172.2
CA-5639 63-29	0.257	192.8	174.4	LF State 4597 5	0.338	196.7	172.8

Table 2 (continued): Saturation values for the 177 superheated wells and the T_o and T_d used to calculated them.

Well Name	So	To (ºC)	Td (ºC)	Well Name	So	To (ºC)	Td (ºC)
CA-5639 63A-29	0.41	197.8	168.9	McKinley 1	0.267	193	173.9
CA-5639 63B-29	0.24	190.6	173.3	McKinley 10	0.307	203.7	182.5
CA-5639 85-28	0.215	188.9	173.3	McKinley 11	0.237	197.7	181
CA-5639 85A-28	0.206	187.8	172.8	McKinley 12	0.24	192.4	175.2
CA-956A 56-34	0.298	194	172.7	McKinley 13	0.287	195.6	175.2
CA-956A 56C-34	0.313	198.3	186.6	McKinley 15	0.42	190.8	177.9
CA-956A 86-34	0.172	200.4	188.4	McKinley 3	0.298	201	180.2
CA-956A 86-34	0.284	193.7	173.4	McKinley 4	0.296	204	183.6
CA-958 37-34	0.309	197	175.2	McKinley 9	0.305	201.9	180.7
CA-958 37A-34	0.209	196.5	181.7	MLM 1	0.276	205	186
CA-958 37B-34	0.226	198.2	182.3	MLM 2	0.292	205	184.9
CA-958 37C-34	0.268	194	181.7	Modini 1	0.267	206.1	187.8
CA-958 56A-34	0.222	193	177.1	Modini 3	0.267	206.1	187.8
CA-958 56B-34	0.318	194.8	172.2	Modini 4	0.365	198.9	173.3
CA-958 86A-34	0.36	198.7	173.4	Ottoboni St 4596 13	0.231	190.6	173.9
CMHC 5	0.168	187.8	175.6	Ottoboni St 4596 14	0.153	185.6	174.4
Coleman 1A-5	0.246	204.2	187.2	Ottoboni St 4596 16	0.174	185	172.2
D & V 1	0.327	194.4	171.1	Ottoboni St 4596 18	0.219	187.2	171.2
D & V 11	0.261	190	171.1	Ottoboni St 4596 23	0.27	190.6	171.1
D & V 12	0.387	198.9	171.7	Ottoboni St 4596 24	0.229	186.7	170
D & V 13	0.352	195.6	170.6	Ottoboni St 4596 29	0.182	187.2	173.9
D & V 15	0.288	192.8	172.2	Sulphur Bank 10	0.245	177.8	159.4
D & V 16	0.295	192.8	171.7	Sulphur Bank 11	0.327	186.1	162.2
D & V 2	0.285	206.7	187.2	Sulphur Bank 14	0.221	177.2	160.6
D & V 6	0.22	182.8	170	Sulphur Bank 17	0.421	188.9	158.4
D & V A-2	0.478	202	168.8	Sulphur Bank 20	0.289	187.2	166.1
D & V A-3	0.437	202	171.6	Sulphur Bank 21	0.203	182.2	167.2
D & V A-4	0.44	199.9	169.1	Sulphur Bank 22	0.249	185	166.7
DX State 4596 22A	0.516	208.9	173.9	Sulphur Bank 23	0.355	192.2	166.7
DX State 4596 23	0.287	193.3	172.8	Sulphur Bank 24	0.379	197.8	171.1
DX State 4596 25	0.247	190.6	172.8	Sulphur Bank 26	0.213	187.2	171.7
DX State 4596 27	0.206	187.8	172.8	Sulphur Bank 27	0.262	190.6	171.7
DX State 4596 4	0.26	188.3	169.4	Sulphur Bank 28	0.225	190.6	174.4
DX State 4596 40	0.232	191.1	174.4	Sulphur Bank 30	0.266	187.2	167.8
DX State 4596 41	0.224	191.1	175	Sulphur Bank 31	0.216	190	174.4
DX State 4596 42	0.332	197.8	174.4	Sulphur Bank 8	0.358	185.6	159.4
DX State 4596 50	0.223	200.6	185	Thorne 1	0.222	199	183.4
DX State 4596 56	0.209	186.4	171.1	Thorne 6	0.27	197	177.9
DX State 4596 58	0.288	194.4	173.9	Tocher 3	0.303	197	175.6
DX State 4596 59	0.305	195	173.3				